Bulletin of the Seismological Society of America, Vol. 94, No. 5, pp. 1644–1657, October 2004

High-Frequency Earthquake Ground-Motion Scaling in Utah and Yellowstone

by Young-Soo Jeon and Robert B. Herrmann

Abstract Velocity seismograms from the University of Utah Seismograph stations are used to quantify high-frequency ground motion scaling for the Yellowstone region and the Wasatch front in Utah. This study uses a data set consisting of over 3000 waveforms from 93 stations and 506 regional earthquakes and mining-associated seismic events that occurred in the years 1995–2001. All events lie within the upper crust with magnitudes less than 5.5. The signals were processed to examine the peak ground velocity and Fourier velocity spectra in the frequency range of 1.0–16.0 Hz. Regression results for Utah are characterized by rapid decreases of amplitude at short distances, which requires low Q and a rapid geometrical spreading $g(r)$ for the forward modeling. $Q(f) = 160f^{0.75}$, $\kappa_{\text{eff}} = 0.05$ sec and $\Delta\sigma = 300$ bars are selected to predict the excitation terms when combined with the derived geometrical spreading. The frequency-dependent excitation of mining-associated events differs significantly from that of earthquakes because of either an additional attenuation due to shallow source depth or apparent low stress drops associated with the slow collapse of long tunnels. A $Q(f) = 140f^{0.70}$ and geometrical spreading less rapid than $r^{-1.0}$ at short distance ranges are used to describe the wave propagation distance dependence in the Yellowstone region. The Yellowstone attenuation functional $D(r, f)$ is very different from that of Utah, perhaps because a shallow wave guide in the caldera traps more energy. The Yellowstone excitation spectra were modeled using $\Delta\sigma = 30$ bars and $\kappa_{\text{eff}} = 0.04$ sec.

Introduction

The most active present-day faulting in Utah is concentrated along the eastern margins of the Basin and Range province (Best and Brimhall, 1974) along the north–south aligned Wasatch fault zone at the eastern boundary of the Basin and Range Province. This fault zone is considered a significant seismic zone because of the known Quaternary normal fault displacement (Machette *et al.*, 1991; McCalpin and Nishenko, 1996). This zone of intraplate seismicity is known as the Intermountain Seismic Belt (Arabasz *et al.*, 1992; Smith and Arabasz, 1991). No major earthquakes greater than magnitude 6 have occurred on the Wasatch fault during the past century and a half. The need for a quantitative ground motion study in this region is important because of the concentration of major population centers near the Wasatch fault zone.

The Yellowstone Plateau (Yellowstone) covers an area of about 6500 km^2 and includes the Yellowstone National Park. It is located at the northeastern corner of the Snake River Plain, is bounded by 44° to 45° 10′ in latitude and −111° 30′ to −109° 45′ in longitude and is at the intersection of the eastern Snake River Plain tectonic axis and the main belt of active seismicity paralleling the east margin of the Basin and Range province (Christiansen, 2001). A wave propagation study here is of interest because of the high seismic activity in the Intermountain Seismic Belt and because Yellowstone is an active volcano-tectonic province with well known displays of geysers, hot springs, fumaroles, and high heat flow (~ 2.0 Wm^{-2}). Large normal faults associated with crustal extension and widespread earthquake swarms are the main characteristics of the seismotectonic setting in this region (Miller and Smith, 1999).

Ground motion prediction often uses the stochastic method (Boore, 1983), which has been used to successfully model high-frequency S-wave ground motion parameters in California and other regions even with the simple Brune point source model for source spectra. This technique uses the signal duration and spectral amplitude of the motion of interest to make its estimates of peak amplitudes. The technique is useful for predicting expected mean motions but cannot account for phase, directivity, or spatial correlations expected from real earthquakes (Boore, 2003). The predicted spectral amplitudes depend on the source spectra, wave propagation, and local site modification.

The purpose of this work is to quantitatively describe

the regional attenuation of the earthquake and mining-associated high-frequency ground motion in Utah and the earthquake motion in Yellowstone region. To accomplish this, regressions are performed with large data sets that cover a wide range of earthquake size and hypocentral distance to calibrate model-based predictions of excitation and propagation. The ultimate purpose of this regional study is that the derived attenuation and source characteristics be used for constraining the amplitude of strong motion expected from future earthquakes be used for engineering design.

To compare the results of this study of high-frequency ground motion scaling in Utah and Yellowstone with results of similar studies in other regions, we will use the same methodology for data processing and analysis as was used in studies with data sets from southern California (Raoof *et al.*, 1999), northwestern United States (Herrmann and Dutt, 1999), central United States (Herrmann and Malagnini, 1996), southern Great Basin (Yazd, 1993), Mexico (Ortega *et al.*, 2003), Greece and Crete (Pino *et al.*, 2001), the Apennines (Malagnini *et al.*, 2000a), Central Europe (Malagnini *et al.*, 2000b), and the Erzincan Region, Turkey (Akinci *et al.*, 2001).

Researchers such as Boatwright and Choy (1992) argued that the teleseismic spectra of larger intraplate events generally depart from the Brune model and that intraplate events may require two corner frequencies. Atkinson (1993) introduced an empirical two-corner source model in a source spectra study in eastern North America to match the observed sag of spectral amplitudes at intermediate frequencies compared with the Brune model. Later, Atkinson and Silva (1997) and Beresnev and Atkinson (1997, 1998, 1999) showed that the observed spectral shapes for eastern North America can be fit by a stochastic finite-fault model. Because of our use of small to moderate earthquake data to study motions in the 1.0–16.0 Hz frequency range, the details of source spectrum scaling for large earthquakes will not be resolved in our study.

Data Set

The University of Utah Seismograph Stations digitally record earthquakes in the intermountain region of the western United States with focus on earthquake activity in Utah and around Yellowstone National Park in Wyoming and Montana. The region monitored is approximately bounded by latitudes 37° N to 46° N and longitudes 114° W to 109° W. Figure 1 shows the epicenters and station locations providing the waveform data set used in this study. The digital waveforms, distributed through the IRIS DMC, were obtained from seismic stations operated by the University of Utah (Utah), the U.S. Geological Survey (USGS), Snow College (SNOW), the U.S. Bureau of Reclamation (USBR), and the Lawrence Livermore National Lab (LLNL). The deployed seismometer systems consist of analog-telemetry short-period single and multicomponent sensors and modern digital telemetry broadband multicomponent sensors.

The data set for analysis consists of 2662 vertical and horizontal component waveforms from 283 regional earthquakes and mining-associated events recorded in the 1998–2001 period for the Utah region and 726 vertical and horizontal component waveforms from 223 earthquakes recorded for the 1995–2000 period in the Yellowstone region. The observations in Utah and Yellowstone cover a hypocentral distance range out to 500 km and 105 km, respectively. All events have shallow focal depths (typically less than 16 km for Utah and 5 for Yellowstone) and have local magnitudes less than 5.0 except for the 21 April 2001 (17:18:49, coordinated universal time [UTC]) $\mathbf{M_W}$ 5.3 Idaho earthquake. We use the term mining-associated because these events will be shown to have a typical spectral signature and occur in regions of known mining.

Data Processing

The data processing procedure is described by Raoof *et al.* (1999) and Malagnini *et al.* (2000a). To study the frequency dependence of ground motion, the digital data are corrected for instrument response to ground velocity in m/sec and each waveform is filtered about a center frequency, f_c, using an eight-pole high-pass causal Butterworth filter with corner frequency at $f_c/\sqrt{2}$ Hz, followed by an eight-pole low-pass Butterworth filter with corner frequency at $\sqrt{2}f_c$ Hz. The center frequencies used are 1, 2, 3, 4, 6, 8, 10, 12, 14, and 16 Hz. The instrument velocity sensitivity of much of the data is roughly constant between 1 and 10 Hz. For each filter frequency, the peak filtered velocity following the *S* arrival, root mean square of Fourier velocity spectra computed in the $(f_c/\sqrt{2}, \sqrt{2}f_c)$ frequency window and duration form the data set for regression.

The observed logarithm of the measured ground motion, $A(r, f)$, of the peak filtered or Fourier velocity is modeled at each frequency by a general regression equation:

$$\log A_{ij}(r, f) = E_i(r, f) + S_j(f) + D(r, f), \qquad (1)$$

where r is the hypocentral distance, i is the source index $(1 \le i \le I)$, j is the site index $(1 \le j \le J)$, $E_i(r, f)$ is the excitation term, and $S_j(f)$ represents the site term. $D(r, f)$ is a piecewise linear function (Yazd, 1993; Anderson and Lei, 1994; Harmsen, 1997) used to represent the distance dependence at a fixed frequency, f:

$$D(r, f) = \sum_{k=1}^{n} L_k(r) D_k \qquad (2)$$

where n is the number of nodes, $L_k(r)$ is a linear interpolation function, and the $D_k \equiv D(r_k, f)$ are node values. The number of nodes and distances are chosen to give a good sampling in the log space in such a manner that sufficient observations lie within each pair of nodes. This linear system can be solved by a least-squares inversion using a singular value

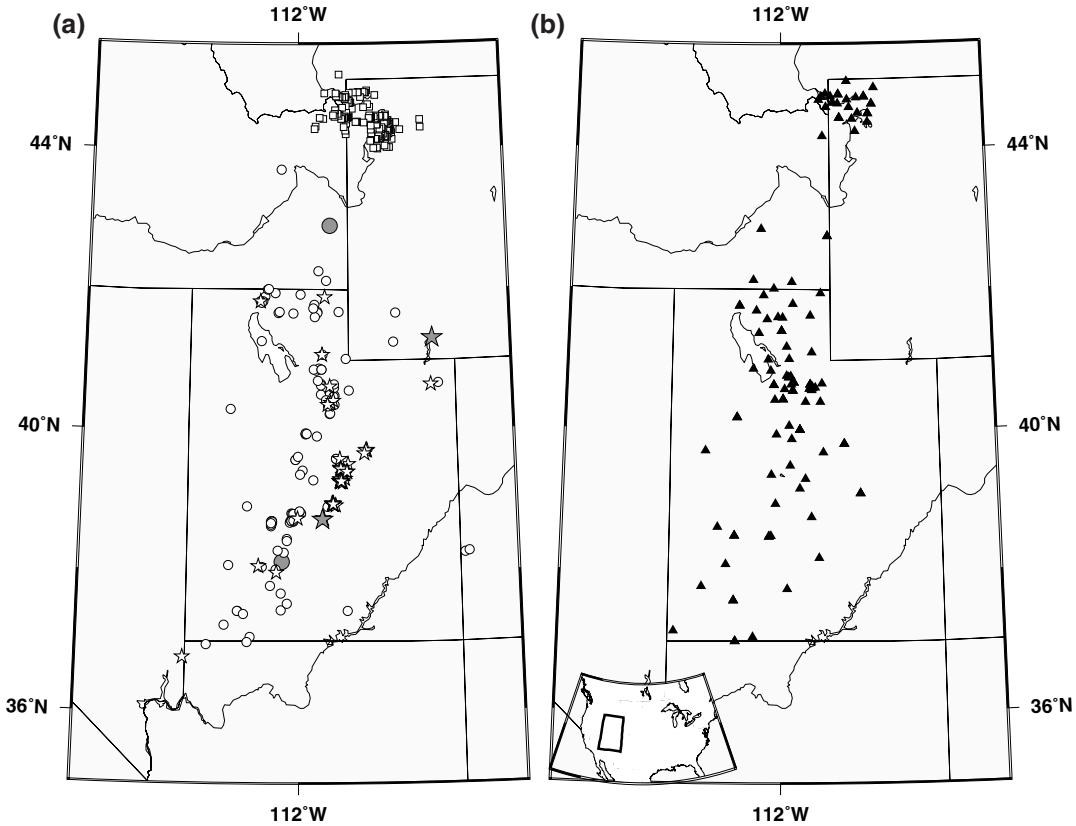

Figure 1. Map shows the epicenters and station locations for the University of Utah dataset. The earthquake epicenters are marked by gray circles and mining-associated events are indicated by stars. Yellowstone events are represented by squares. The gray circles and stars indicate the epicenters of known moment magnitudes (a). Stations are denoted by black triangles (b).

decomposition algorithm (Lawson and Hanson, 1974). The following constraints are used in this study to reduce the number of degrees of freedom of the system to permit a stable inversion:

- $D(r_{\mathrm{ref}}) = 0$, where $r_{\mathrm{ref}} = 40$ km.
- $\Sigma\, S_j(f) = 0$ for selected data channels, and
- A smoothing constraint applied to the $D(r)$: $D_{k-1} - 2D_k + D_{k+1} = 0$ (Malagnini *et al.*, 2000a).

Given the level of motion $E_i(r_{\mathrm{ref}}, f)$ at $r_{\mathrm{ref}} = 40$ km, the $D(r, f)$ propagates that motion to the desired distance, r, and the site term adjusts that motion to a particular physical location.

As a check on the regression we applied the coda normalization technique (Aki, 1980; Frankel *et al.*, 1990) to provide an independent estimate of the $D(r, f)$ that should be free of concerns about instrument response and unknown source and site effects, as long as these do not change with time. The coda normalization technique consists of dividing the amplitude of the peak motion by the coda level, thus accounting for the instrument gain, source excitation, and site amplification effects. The coda derived $D(r, f)$ estimate is not used for forward modeling but only as a starting point for the inversion (equation 2). Because our data sets consist of vertical (Z) and horizontal (H) channels, we perform several regressions: Z only, H only, and Z and H with site constraints $\Sigma\, S_Z = 0$, $\Sigma\, S_H = 0$, and $\Sigma\, S_Z = 0$, respectively.

Interpretation

Because the objective of the study is to parameterize observed ground motions in a manner that permits a forward prediction using random vibration theory or band-limited Gaussian noise (Boore, 1983), the specification of ground motion spectra and duration at the site is required. An equation for the predicted Fourier velocity spectra at a frequency f for a hypocentral distance r is

$$A(r, f) = S(f, \mathbf{M_W})\; g(r)\; e^{-\pi f r / Q(f)\beta}\; V(f) e^{-\pi f \kappa} \qquad (3)$$

where $A(r, f)$ is the Fourier velocity spectrum, $S(f, \mathbf{M_W})$ is the Fourier velocity spectrum at a distance of 1 km, $\mathbf{M_W}$ is the moment magnitude, $g(r)$ is the geometrical spreading function relative to 1 km, and $Q(f)$ is the frequency-dependent quality factor which is taken to be $Q_0\,(f/1.0\ \mathrm{Hz})^{\eta}$ and β is the shear-wave propagation velocity. The combination

of $V(f)$ and κ characterizes the frequency-dependent site amplification.

A comparison of this simple prediction model with the regression terms (equations 1 and 2) shows the following correspondence with the excitation, propagation, and site terms:

$$10^{E} = S(f, \mathbf{M_W})\ g(r_{\mathrm{ref}})\ e^{-\pi f_{\mathrm{ref}}/Q(f)\beta}\ \overline{V(f)e^{-\pi\kappa f}}, \quad (4)$$

at $r = r_{\mathrm{ref}}$,

$$10^{D} = \frac{g(r)\ e^{-\pi f r/Q(f)\beta}}{g(r_{\mathrm{ref}})\ e^{-\pi f r_{\mathrm{ref}}/Q(f)\beta}}, \quad (5)$$

and

$$10^{S_i} = \frac{V(f)e^{-\pi\kappa f}}{\overline{V(f)e^{-\pi\kappa f}}}, \quad (6)$$

where $\overline{V(f)e^{-\pi\kappa f}}$ is the network average site effect. Since we know little about the sites, we define an effective κ, κ_{eff}, for the composite effect of network average site amplification, $V(f)$ and κ by the relation:

$$e^{-\pi f \kappa_{\mathrm{eff}}} = \overline{V(f)e^{-\pi\kappa f}}. \quad (7)$$

Note that if $V(0) = 1$, both sides of the equation approach 1.0, but that there may be a constant multiplier in equation (7) when only a limited range of frequencies is used and there is some site amplification.

As a result of interpreting the regression results and constraints in terms of this conceptual forward model, we characterize the excitation term, E, as the expected network average motion at the reference hypocentral distance for a given event, the D term as a function that projects this motion to the hypocentral distance of interest, r, and the S_i term as one that relates a specific site to the network average site response. The regression results are purely empirical and the forward model does not predict absolute motions unless there is some independent calibration.

Wave Propagation in Utah and Yellowstone

Data processing of the observed data sets of peak filtered velocity and Fourier velocity spectra yields the $D(r, f)$, $S(f)$, and $E(r, f)$ terms and an estimate of the signal duration, $T(r, f)$. Forward modeling of the data-derived parameters is done sequentially, using the interpretations of the regression terms as given by equations (4)–(6). First the Fourier velocity spectra $D(r, f)$ are modeled using (5) by interactively specifying $g(r)$ and $Q(f)$. Because of the limited distance and frequency range in any observational data set, there will be trade offs between these two parameters and the interdependence of the $g(r)$ and $Q(f)$ is acknowledged by presenting both. The $g(r)$ and $Q(f)$ are used with the $T(r, f)$ to make random vibration theory (RVT) predictions (Cartwright and Longuet-Higgins, 1956; Boore, 2003) of the filtered peak time domain $D(r, f)$ as a check on the internal consistency of these three parameters.

We next focus on the $E(r, f)$ term for small earthquakes. The predicted $E(r, f)$ does not depend on the source spectrum details for the very small events in our data set for which the source corner frequencies are greater than our observations. From equation (4), we see that in this case the observed $E(r, f)$ frequency-dependent shape depends only on the already determined $Q(f)$ and $g(r)$ and the network average site effect, which we model in terms of the κ_{eff} in equation (7).

The final step is an attempt to define the absolute scaling of ground motion by predicting the observed $E(r, f)$ for larger events. This step requires the use of an event large enough to have a surface-wave-defined moment magnitude estimate, for example, $\mathbf{M_W} > 4.0$ event, but also small enough that the excitation is insensitive to stress drop in the lower frequency range. This step permits a check on the assumed $g(r)$ from the source to the first observational data distance that is otherwise not constrained and also the assumed average source radiation pattern (Herrmann and Malagnini, 2004). If all these steps are successful, we will claim that we have a model that explains the observed data set and also should form the basis for extrapolating vertical and horizontal motions to larger events once the large earthquake source scaling is specified.

Regression Results

Figure 2 shows a typical example of the regression analysis result for the peak bandpass-filtered ground velocities for the Utah region at filter frequencies of 1.0 and 4.0 Hz. The top panels show the $D(r, f)$ term estimated by the coda normalization technique. The gray line represents the attenuation functional computed by a linear interpretation between each nodal point (Malagnini *et al.*, 2000a). The middle panels compare the coda and regression distance functionals which indicate good agreement at all distance ranges at 1.0 Hz and at most distances for 4.0 Hz. The regression residuals at the bottom show that the distance nodes used are appropriate to determine $D(r, f)$. Note that there are only a small number of observations at distances less than 20 km.

Figure 3 is an example of the regression analysis results for the Yellowstone region for the peak bandpass-filtered ground velocities at frequencies of 1.0 and 4.0 Hz. The coda propagation functional estimated by the coda normalization technique (top) and propagation function (middle) regression results show a reasonable agreement. The network geometry and the lack of larger events limit the data set to distances less than 105 km. Although the hypocentral distance range is narrower, more observations are used to validate the near distance range of $D(r, f)$ than was possible for Utah. The distribution of regression residuals also shows less scatter than those of Figure 2 for Utah.

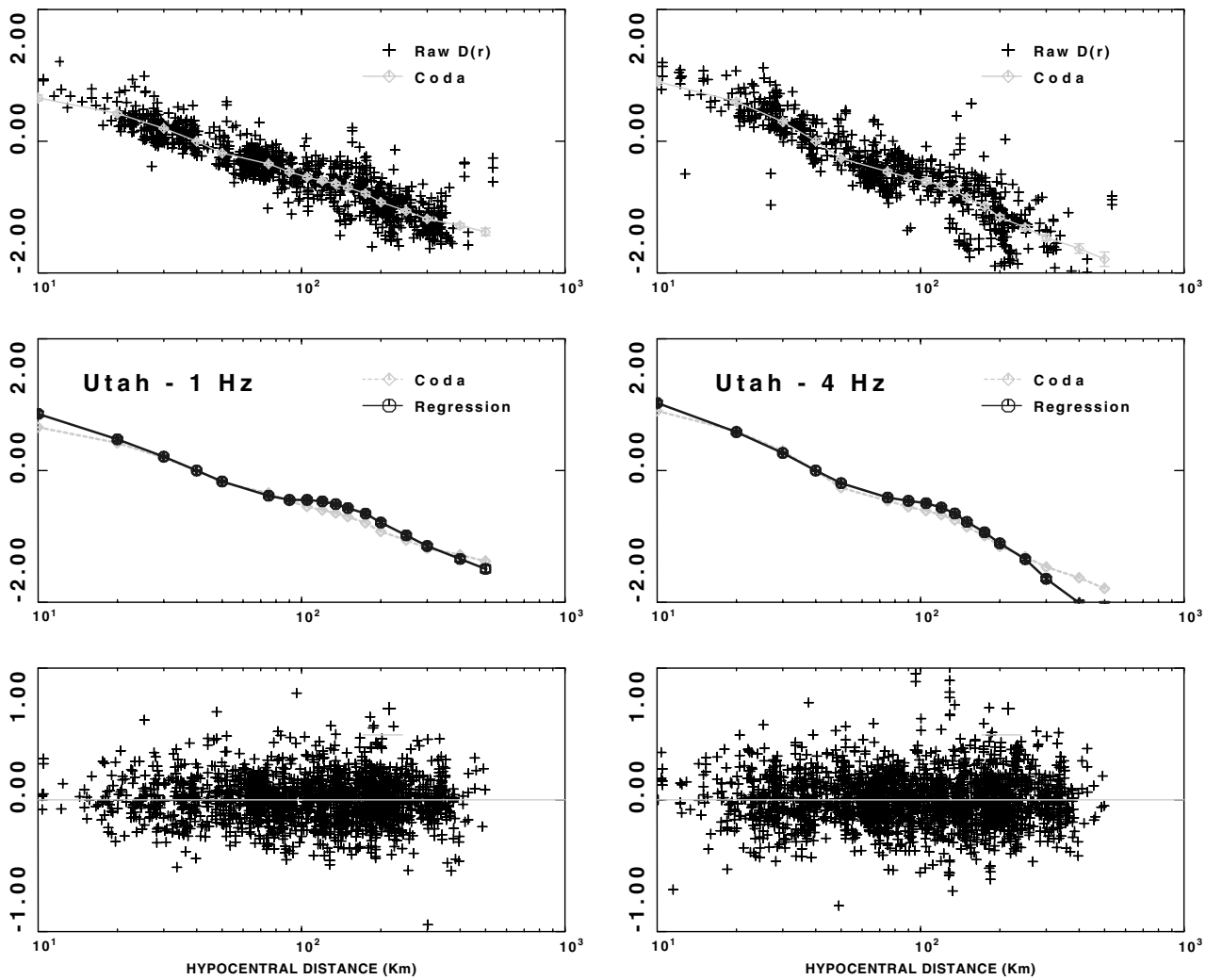

Figure 2. Regression analysis results at 1.0 (left side) and 4.0 Hz (right side) obtained for the Utah region. (Top) Coda estimate of $D(r)$ (open diamonds linked by thin gray lines) using coda normalization technique. (Middle) Coda and regression propagation functional from the regression on the bandpass-filtered amplitudes (open circles linked by thin black lines). (Bottom) Final residuals as a function of distance.

The regression provides standard error estimates of the $D(r, f)$, $E(r_{\mathrm{ref}}, f)$, and $S(f)$. The estimates of the standard errors of the residuals are shown in the bottom frames of Figures 2 and 3. For the Utah data set, the number of observations shown in Figure 2 vary from 2000 at 1 Hz, to 2500 at 10 Hz to 2300 at 16 Hz. The standard error describing the residuals varies from 0.18 to 0.25 $\log_{10}$ units. The standard errors of the $D(r)$ are less than 0.06 at all frequencies for distances less than 500 km. The error on $D(500, 16)$ increases to 0.08, which reflects the small number of observations near this distance. The standard errors on the $S(f)$ terms are usually less than 0.1 $\log_{10}$ units, whereas that of the individual event $E(r_{\mathrm{ref}}, f)$ terms depends on the number of traces used for that event, being less than 0.1 if there are more than 10 observations. The reason that the $D(r)$ errors are so small is related to the fact that all waveform data contribute to its determination, and fewer data define the excitation term. For the Yellowstone data set, the standard error of the residuals varies between 0.16 and 0.18 $\log_{10}$ units. The standard error of the $D(r)$ is less than 0.09 for all distances.

Duration

The application of RVT requires a specification of signal duration. Our duration definition is that of Yazd (1993) and Raoof *et al.* (1999) who defined it in terms of the time window that contains the 5%–75% portion of the cumulative energy following the *S*-wave arrival. Duration is a function of the rupture process and the dispersion or scattering that elastic waves experience along the source to receiver paths. It is assumed to be of the form $T_s + T(r)$, where T_s is the source duration and $T(r)$ is the distance-dependent wave propagation contribution to total duration (Herrmann, 1985). For very small earthquakes, we may assume that $T_s = 0$.

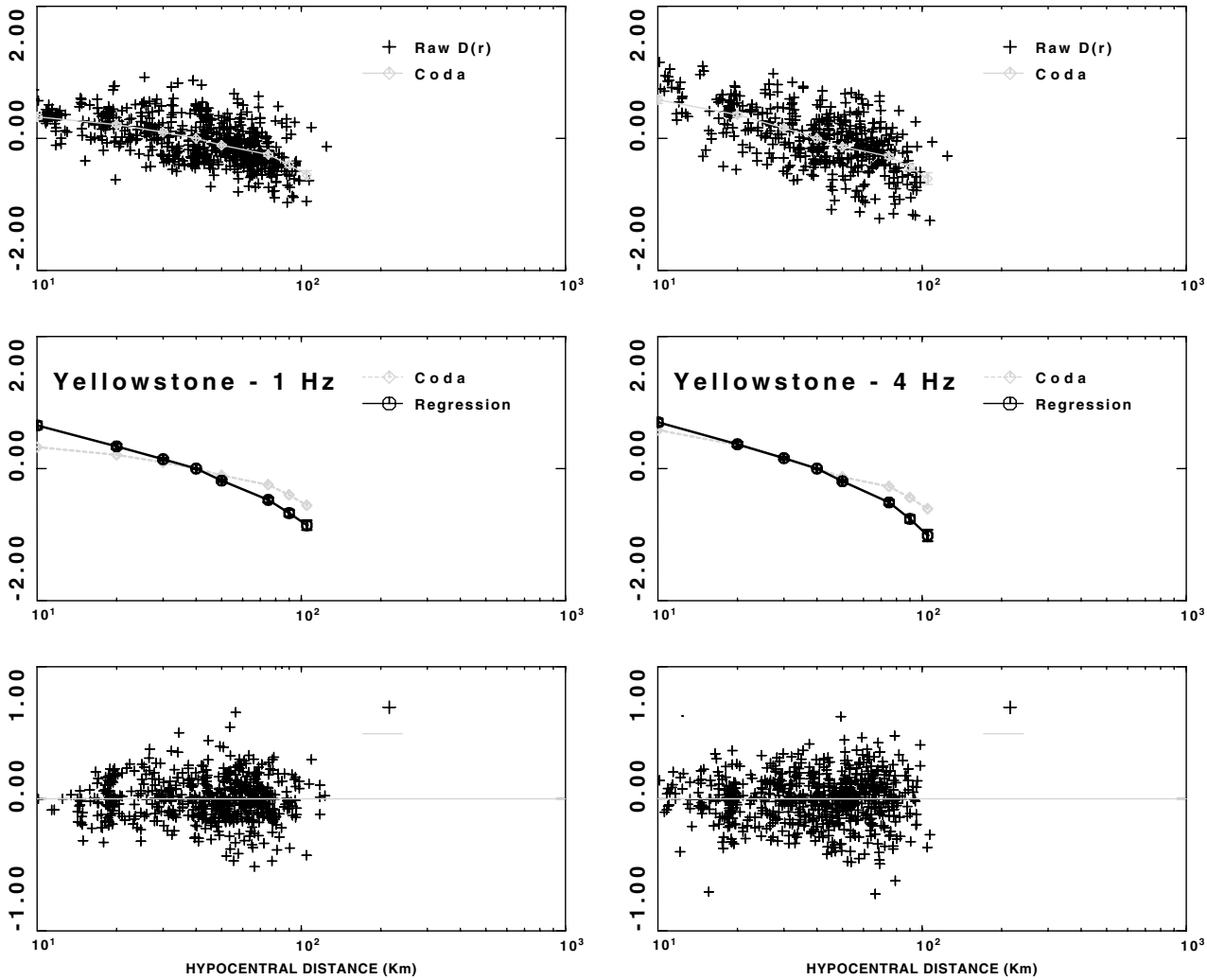

Figure 3. Regression analysis results obtained at 1.0 (left side) and 4.0 Hz (right side) for the Yellowstone region. (Top) Coda estimate of $D(r)$ (open diamonds linked by thin gray lines) using coda normalization technique. (Middle) Coda and regression propagation functional from the regression on the bandpass-filtered amplitudes (open circles linked by thin black lines). (Bottom) Final residuals as a function of distance.

Duration increases with increasing earthquake magnitude, distance, and scattering effect.

Figure 4 shows the measured duration at 1.0, 3.0, 6.0, and 10.0 Hz for the Utah region for the earthquake population. The individual duration estimates (gray circles) show less scatter in a frequency range of 1.0–6.0 Hz, while there is much scatter in the automatic determination of duration at higher frequencies. The durations (thick solid lines) increase with increasing hypocentral distance and decrease with increasing frequency range. This result is similar to the observations of Raoof *et al.* (1999) that low-frequency signals have longer durations than those of higher frequency. Because the high-frequency signals (>10 Hz) are rapidly attenuated, we can only determine the duration out to perhaps 250 km. Following Malagnini *et al.* (2000b), who suggested the use of an $L1$ norm for this determination, we define the $T(r)$ using median values within selected distance bins. These are plotted as solid lines in each figure frame. As will be seen in the section on the excitation terms, the original event set had two distinct types of shapes. Figure 4 shows the durations obtained for the earthquake data set. If we had not done this, there would be a bigger bump near a distance of 75 km because of the observations of shallow mining-associated events by stations at this distance.

Table 1 lists an adequate frequency-independent duration functional as a function of distance for vertical (Z), horizontal (H), and Z and H data sets of Utah and Yellowstone. In determining the durations for Utah, we only used the known earthquakes. If we use the entire data set, which we will show contains events with anomalous excitation, the durations are similar, but with a slightly larger bump at 75 km, a common distance from some known mining areas.

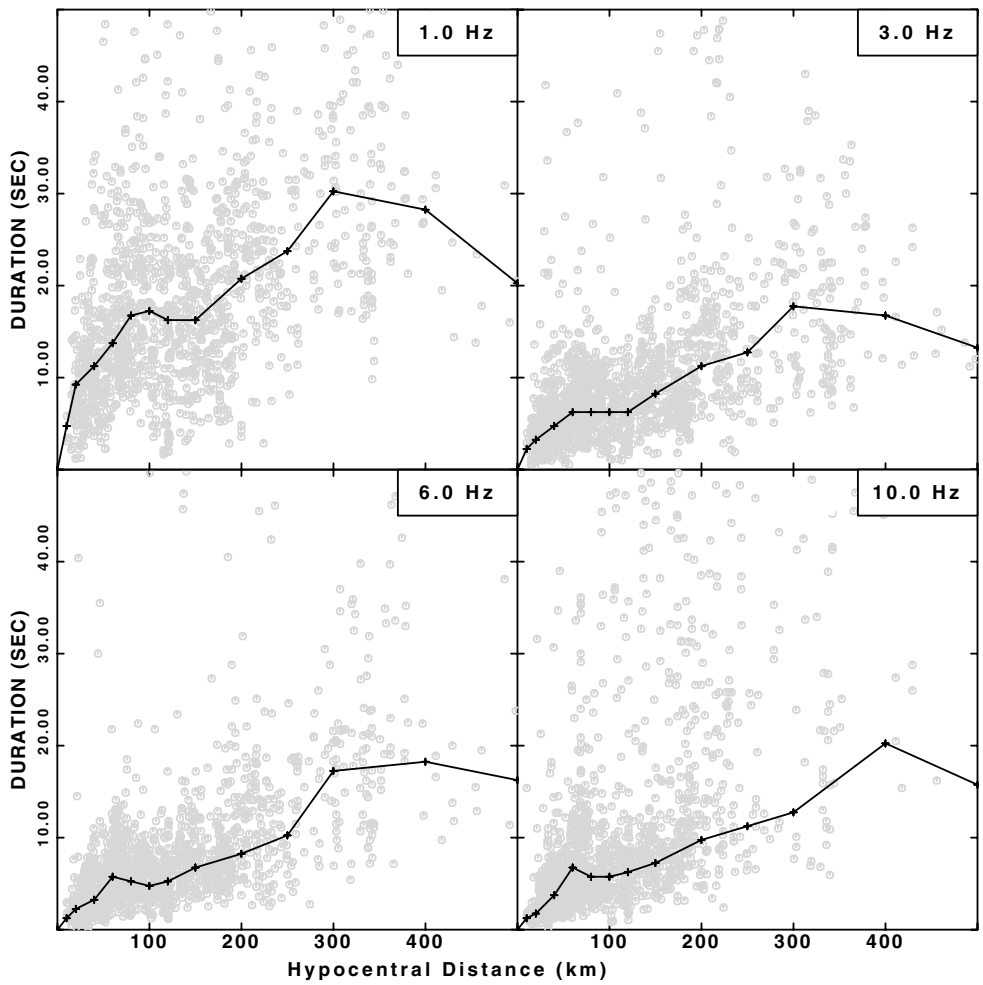

Figure 4. Durations at 1.0, 3.0, 6.0, and 10.0 Hz obtained for Utah region. Rounded gray circles indicate individual duration estimates. Thick solid lines denote the duration using a median value method which is less affected by outliers.

Table 1
Measured Durations for Utah and Yellowstone

Distance (km)	Utah H (sec)	Utah Z (sec)	Utah Z & H (sec)	Yellowstone (sec)
20	2.1	2.9	2.6	2.3
40	4.5	4.4	4.4	3.2
60	8.2	6.6	7.1	5.8
80	7.4	6.6	6.8	5.3
100	5.5	6.4	6.2	5.8
120	6.6	6.5	6.6	—
150	7.9	8.6	8.5	—
200	10.1	11.1	11.3	—
250	12.0	13.4	13.9	—
300	15.7	15.7	16.7	—
400	16.2	16.7	17.9	—
500	20.0	16.0	15.2	—

Regional Attenuation

Figure 5a compares the Z (vertical) and H (horizontal) combined data set distance scaling of the $D(r, f)$ term for Utah at the ten different frequencies. The regression results on the peak filtered velocities are plotted in gray shades and the theoretical predictions as solid black curves. The theoretical attenuation modeling (black curves) is first defined by fitting the Fourier velocity $D(r, f)$ by determining $g(r)$ and $Q(f)$ and then tested through using the measured duration and RVT to match the time domain $D(r, f)$. The plot emphasizes the departure from r^{-1} spreading. Because the Fourier velocity and peak filtered $D(r, f)$ regression results are characterized by rapid decreases of amplitude at distances less than 40 km, we required a geometrical spreading slightly more rapid than r^{-1} (Malagnini and Herrmann, 2000; Atkinson, 2004) in the 10- to 50-km distance range rather than the typical geometrical spreading often assumed by other investigators. Figure 5b shows the bandpass-filtered $D(r)$ residuals, the deviation between observed and predicted $D(r, f)$ of the distance range. The residuals of fit are less

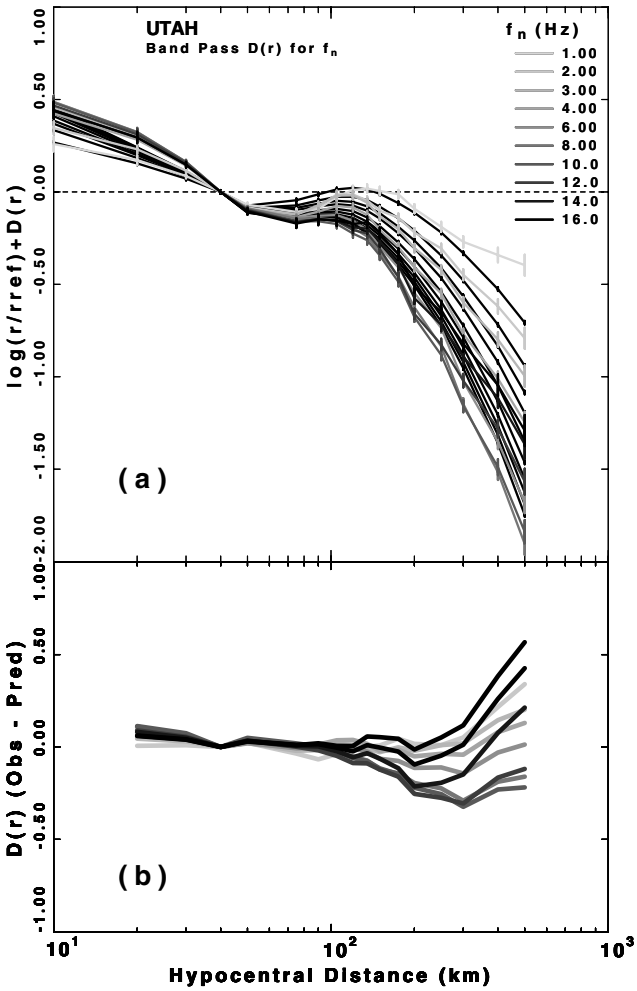

Figure 5. (a) The reduced attenuation functional $D(r, f)$ obtained from the regression on the bandpass-filtered velocities at the frequencies of 1.0, 2.0, 3.0, 4.0, 6.0, 8.0, 10.0, 12.0, 14.0, and 16.0 Hz for the Utah region. This $D(r, f)$ is obtained from the regression of vertical and horizontal component data sets. The black lines in the background are the theoretical $D(r, f)$. The reference distance at 40 km was used to normalize the $D(r, f)$. The presentation of this plot is to emphasize the departure from r^{-1} spreading. The horizontal dashed line represents r^{-1} trend. (b) The residuals of the model fit to the band pass $D(r, f)$ for the frequency range of 1–16 Hz.

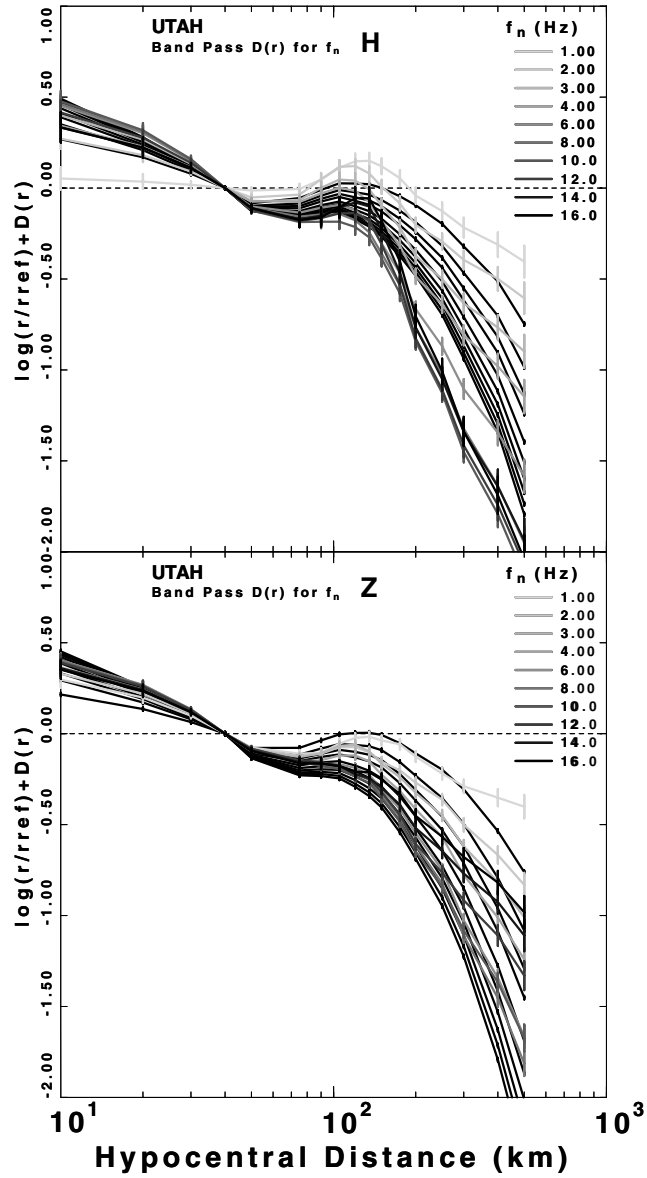

Figure 6. Horizontal component (top) and vertical component (bottom) reduced the attenuation functional $D(r, f)$ obtained from the regression on the bandpass-filtered velocities of 1.0, 2.0, 3.0, 4.0, 6.0, 8.0, 10.0, 12.0, 14.0, and 16.0 Hz for the Utah region. The black lines at the background are the theoretical $D(r, f)$. The reference distance at 40 km was used to normalize the $D(r, f)$. The presentation of this plot is to emphasize the departure from r^{-1} spreading.

than 0.1 out to 150 km, but they increase in a manner that is not simply related to frequency dependence at larger distances. We could not find a simple model that reduced the deviation at larger distances.

Figure 6 shows horizontal (top panel) and vertical (lower panel) component distance scaling of the $D(r, f)$ terms for the separate regressions on the peak filtered velocities for Utah. Both $D(r, f)$ have an amplitude decay similar to the $D(r, f)$ of Figure 5a, except at the lowest frequency. The low-frequency horizontal component $D(r, f)$ shows less amplitude decay at short distances and has a more pronounced shoulder or bump near a hypocentral distance of 150 km. This may be due to the smaller number of waveforms used for the estimation or the effect of noise at 1 Hz signal. The number of traces used for the horizontal component regression are 972, and 1690 are used for the vertical component signal processing. We used same model parameters except for different $g(r)$ at a short distance range and separate durations for each component. An $r^{-1.1}$ is required to fit the distance range (10–50 km) for vertical component,

whereas $r^{-1.2}$ is used to fit the horizontal component distance scaling (10–50 km).

Figure 7a compares the frequency dependence of the $D(r, f)$ for the Yellowstone data set. The attenuation functional is only defined out to 105 km because of the lack of observations at greater distances. This $D(r, f)$ shows a less rapid decrease of amplitude at short distances than observed in Utah (Fig. 5) and in other studies with observations in the same distance range (Malagnini *et al.*, 2000a, b; Raoof *et al.*, 1999). Figure 7b shows the residual of our model fit for the observed bandpass-filtered $D(r, f)$ as a function of distance. The $D(r)$ residual plot shows that the forward model predicts the $D(r)$ to within 0.1 for distances less than 90 km, with a increasing lack of fit at larger distances, for which we had fewer observations.

Tables 1 and 2 list the parameters used to compute the theoretical propagation models for the Utah and Yellowstone regions. We emphasize that the $Q(f)$ must not be used independently of the $g(r)$, because the combination of the two is required to fit the observations and cannot be separated because of the limited frequency and distance ranges in the processed data set.

Site Terms

Figure 8 shows the site terms for the Yellowstone (top two panels) and Utah (bottom two panels) data sets for the regressions on the peak filtered velocity values. The individual Utah and Yellowstone site terms agree well among themselves. To obtain this agreement we deleted a few stations having only a few observations. We note that one extremely poor observation, because of incorrect station calibration or the small number of data, can cause the site terms to trade off with the excitation spectral levels. We thus permit those stations with large numbers of observations to have the primary influence on the results. Figure 8b is an example of the effect of using a small number of data in the regression. Only 197 horizontal component waveforms are used for the horizontal component site terms of Yellowstone, whereas 726 vertical and horizontal component waveforms are used to obtain the site terms of Figure 8a.

Excitation Terms

The theoretical Fourier velocity spectra at a distance of $r = 1$ km used in (3) is

$$S(f, \mathbf{M_W}) = \frac{C\ M_0\ 2\pi f}{(1 + (f/f_c)^2)} \tag{8}$$

where the seismic moment in dyne-cm is a function of moment magnitude $\mathbf{M_W}$ and f_c is the source corner frequency (equation 4; Boore, 2003) defined in terms of S-wave velocity β (in km/sec), M_0, and a stress propagation parameter $\Delta\sigma$. The constant C is

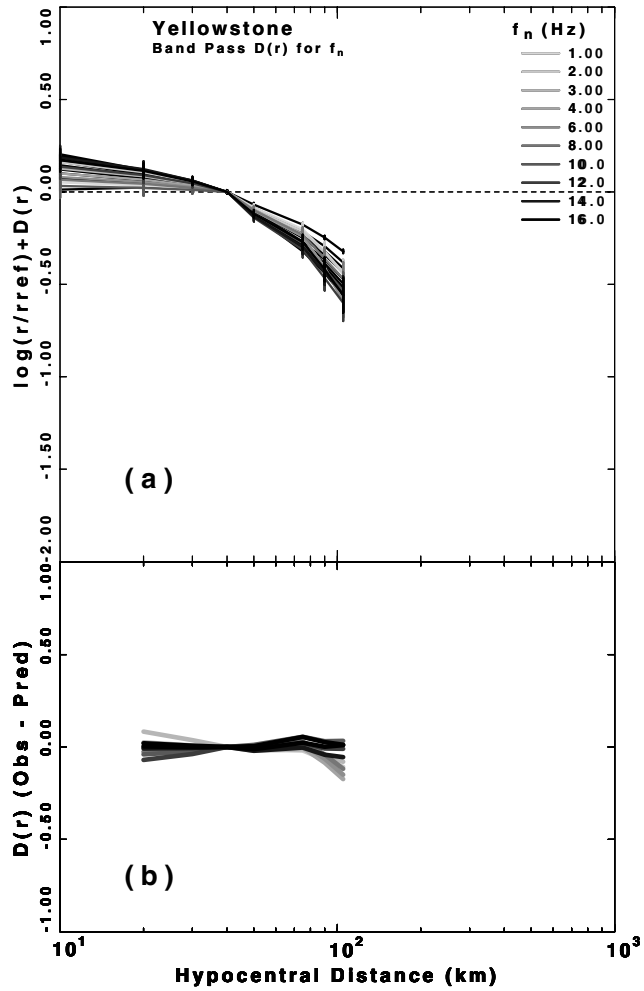

Figure 7. (a) The attenuation functional $D(r, f)$ obtained from the regression on the bandpass-filtered velocities at the frequencies between 1.0 and 16.0 Hz for the Yellowstone region. The $D(r, f)$ obtained from the regression of vertical and horizontal component data sets. The black lines in the background are the theoretical $D(r, f)$. The reference distance at 40 km was used to normalize the $D(r, f)$. (b) The residuals of the model fit to the bandpass $D(r, f)$ for the frequency range of 1–16 Hz.

Table 2
Propagation Parameters of Utah and Yellowstone

Parameter	Utah		Yellowstone	
$Q(f)$	$160f^{0.75}$		$140f^{0.70}$	
$g(r)$	$r^{-1.2}$	$0 < r \leq 50$ km		
	$r^{-0.55}$	$50 \leq r \leq 60$ km	$r^{-0.80}$	$0 \leq r \leq 40$ km
	$r^{-0.2}$	$60 \leq r \leq 90$ km	$r^{-1.1}$	$40 \leq r \leq 80$ km
	$r^{-0.1}$	$90 \leq r \leq 140$ km	$r^{-1.4}$	$80 \leq r \leq 105$ km
	$r^{-0.5}$	$140 < r \leq 500$ km		

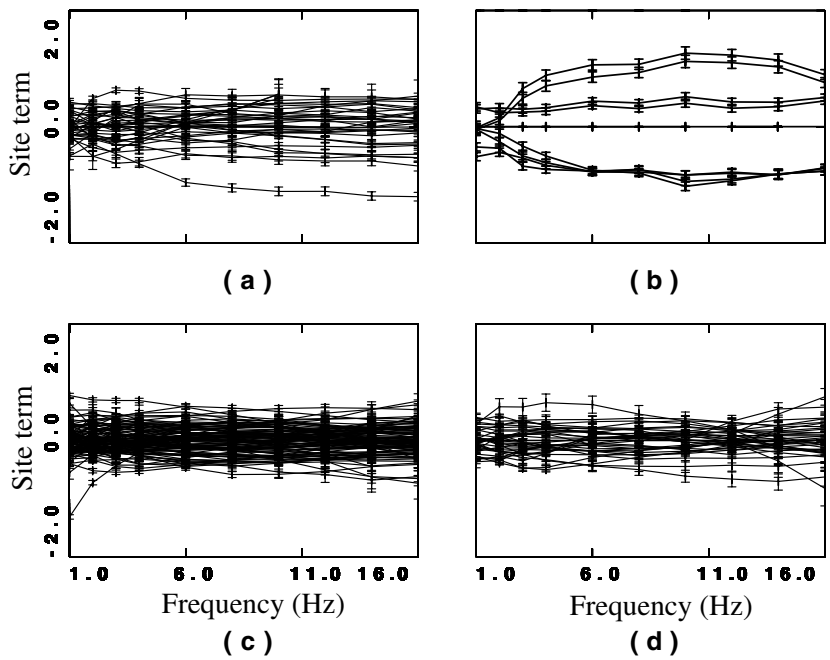

Figure 8. Inverted site amplifications of Yellowstone (a and b) and Utah (c and d) in peak amplitudes. a and c are Z (vertical) and H (horizontal) component site terms of ground motion, and b and d are H component site terms of ground motion. The constraint of $\Sigma S_Z(f) = 0$ is used for site amplifications on a and c, and the constraint of $\Sigma S_H(f) = 0$ is used for site amplifications on the b and d.

$$C = \frac{R_{\Theta\Phi}\ FV}{10^{20}\ R_0\ 4\pi\rho\beta^3}. \tag{9}$$

Here, $R_{\Theta\Phi}$ represents the radiation pattern averaged over a suitable range of azimuths and takeoff angles, F is the amplification at the free surface, V is the reduction factor that accounts for the partitioning of energy into two horizontal components, R_0 is a reference distance set equal to 1 km, ρ is the density (in g/cm^3) at the source, and 10^{20} converts kilometers to centimeters so that M_0 has units of dyne-cm and $S(f, \mathbf{M_W})$ has units of cm-sec. We use $R_{\Theta\Phi} = 0.55$, $F = 2.0$, $V = 0.707$ according to Boore (2003).

Figure 9 shows the Fourier acceleration spectra at a distance 1 km for six different moment magnitudes and five stress parameters, 10, 30, 100, 200, and 400 bars. For $\mathbf{M_W}$ 2, there is a little dependence of shape of the spectrum between 1.0 and 16.0 Hz as a function of the stress parameter. For $\mathbf{M_W}$ 4, the spectral shape in this passband is very dependent on the stress parameter except at frequencies less than 1.0 Hz. This means that the shape of the excitation $E(r, f)$, depends only on the $Q(f)$ and κ_{eff} for the very small event data. Because of this, the study of small earthquakes enables us to estimate the network average site effect without worrying about the effects of unknown source spectrum scaling. In equation (7), we fixed $V(f) = 1$ and varied κ_{eff} to fit the observed excitation for the small events.

Figure 10 compares the observed and predicted excitation of filtered velocity spectra obtained from the Utah region. The black lines indicate the regression results, and the thick gray lines denote the theoretical excitations computed by equation (4). We found that a $\kappa_{\text{eff}} = 0.05$ sec is required to fit our data and that $\Delta\sigma = 300$ bars fits the observed $E(r, f)$ over 3 orders of magnitude. We determined an $\mathbf{M_W}$ 5.2 and an oblique normal fault mechanisms (Table 3) for the Idaho earthquake by examining regional surface-wave amplitude spectra patterns using the technique of Herrmann (1979). This result is similar to the CMT catalog result, $\mathbf{M_W}$ 5.3 (www.seismology.harvard.edu/CMTsearch.html). The theoretical excitation level of $\mathbf{M_W}$ 5.0 in Figure 10 almost matches the excitation for the Idaho earthquake magnitude (the thin black line at the top linked by the thick long-dashed line). The purpose of comparing the known moment with the spectral level of the theoretical excitation is to check whether our model-based parameters are appropriately selected to predict the theoretical excitation spectra, especially the chosen geometrical spreading $r^{-1.2}$ at short distance range. The Idaho earthquake's source excitation level lies between the theoretical excitation levels of $\mathbf{M_W}$ 5.0 and $\mathbf{M_W}$ 5.5, and this suggests that our model parameters are appropriate to describe the ground motion in Utah region. We studied another event (2 January 1998) by examining regional surface-wave amplitude spectra patterns (Hermann, 1979) and determined an $\mathbf{M_W}$ 4.5. The source excitation of that event lies below the Idaho earthquake's excitation (the thin black line at the top linked by the thick short-dashed line) and its level matches with the theoretical spectral level of $\mathbf{M_W}$ 4.5. The two gray circles in Figure 1 indicate the epicenters of Idaho (42°92′ N, 111°39′ W) and another (38°18′ N, 112°46′ W) event.

In our initial review of the excitations, we noticed another distinct shape for the excitation terms (Fig. 11). Because of concern about the effect of anomalous sources on regression, we removed these events from the data set and redid the initial regression for earthquake $D(r, f)$ with no major differences. The excitation of events in Figure 11 shows a rapid fall-off of high-frequency spectra. We applied

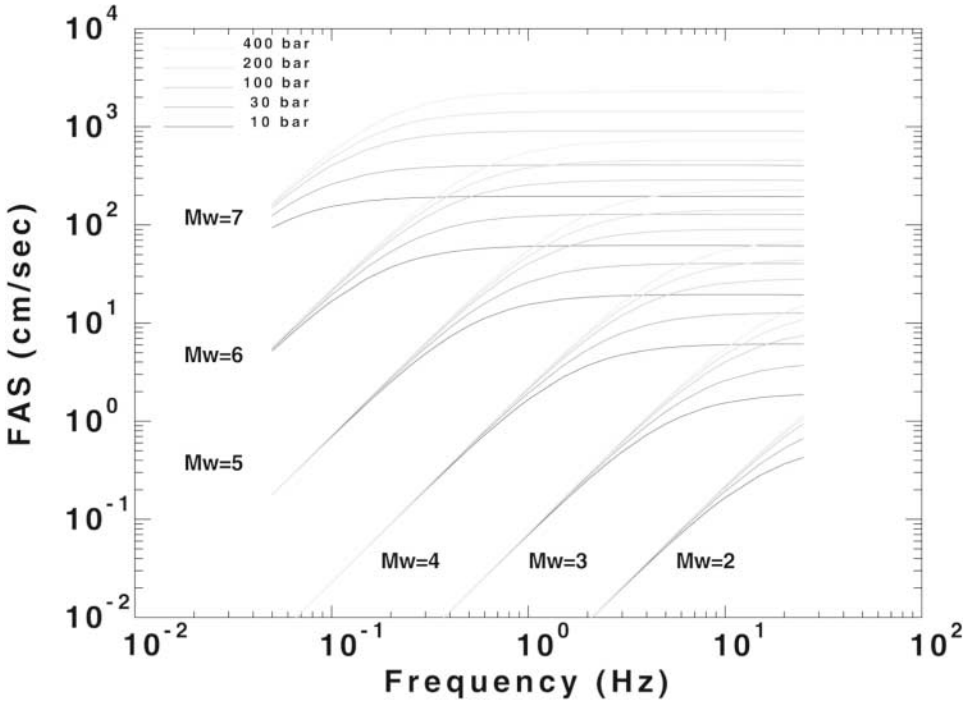

Figure 9. Fourier acceleration spectra at a distance of 1 km as a function of $\mathbf{M_W}$ for stress drop of 10, 30, 100, 200, and 400 bars. Darkest to lightest lines indicate 10 to 400 bars stress drop. The different $\mathbf{M_W}$ values are indicated by the different low-frequency asymptotes. For a given $\mathbf{M_W}$, the high-frequency level varies as $\Delta\sigma$.

different stress drops to match the observed spectra with theoretical spectra, but none of them fit the entire excitation spectra. There is a better fit with the low stress drop event at the indicated moment magnitudes, but these stress drops may not be the true values.

Two of the anomalous events were large enough to have $\mathbf{M_W}$ determined by regional surface-wave amplitude spectra patterns (Fig. 11). The $\mathbf{M_W}$ 4.1 event (30 January 2000) and $\mathbf{M_W}$ 4.2 event (19 July 2001) are used to check the validity of our theoretical excitation levels with 10-bar stress parameters. The source excitation level of $\mathbf{M_W}$ 4.1 event matches the theoretical excitation level of $\mathbf{M_W}$ 4.0, whereas that of $\mathbf{M_W}$ 4.2 event matches the $\mathbf{M_W}$ 4.5 prediction. Despite the fact that the theoretical spectral levels of those two events match the observed excitations of filtered velocity spectra, the whole excitation shape of Figure 11 cannot be fit by the Brune's model unless much lower stress parameters are used for the smallest events.

The epicenters of the events having the anomalous excitation are indicated in Figure 1 with stars. Note that there is a narrow grouping of these events in Colorado Plateau (about 39° N and 111° W). The two gray stars in Figure 1 indicate the epicenters of $\mathbf{M_W}$ 4.1 event (41°52′, 109°81′) and $\mathbf{M_W}$ 4.2 event (38°73′, 111°52′). Even if the stars in Figure 1 seem to be colocated with known long-wall underground coal mines, a few of them are located outside of the known underground mining area. It is not clear what makes these outliers. Pechmann *et al.* (1995) indicated from the study of the 3 February 1995 $\mathbf{M_L}$ 5.1 southwestern Wyoming event that the event was caused by underground collapse and differed from conventional earthquakes by lack of Love wave excitation. The epicenter of the 1995 Trona mine event (41°31′, 109°48′) is close to that of the $\mathbf{M_W}$ 4.1 event. The focal depth of the $\mathbf{M_W}$ 4.1 event is 7 km, whereas that of the 1995 event is 4 km, which is the arbitrarily fixed depth to compute the hypocenter relocation and any fixed focal depth shallower than 10 km fits arrival time data well (Pechmann *et al.* 1995). But, the epicenter and focal depth (2.0 km) of our $\mathbf{M_W}$ 4.2 event is different from that of the 1995 event even if the spectral shapes of $\mathbf{M_W}$ 4.1 and $\mathbf{M_W}$ 4.2 are similar. The complicated spectral shapes of Figure 11 may be diagnostic of collapse-related sources. Table 3 summarized the results of the focal mechanism that we studied.

Figure 12 shows the excitation of peak filtered velocity as a function of frequency for the Yellowstone region. To determine κ, we fit average excitation values. An $\kappa_{\text{eff}} = 0.04$ sec is selected to match the high-frequency shape of the ground excitation terms. The kappa value trades off with other parameters such as geometrical spreading that controls the level of the spectrum and stress drop which adjusts the shape of low- to middle-frequency spectral range (above 1 Hz). The Yellowstone study is limited because of a lack of large earthquakes and a wave propagation distance range limited to 105 km. Even if our predicted excitation shapes matched the observed excitation, the corresponding moment magnitudes are 0.5 to 1.0 units smaller than the University

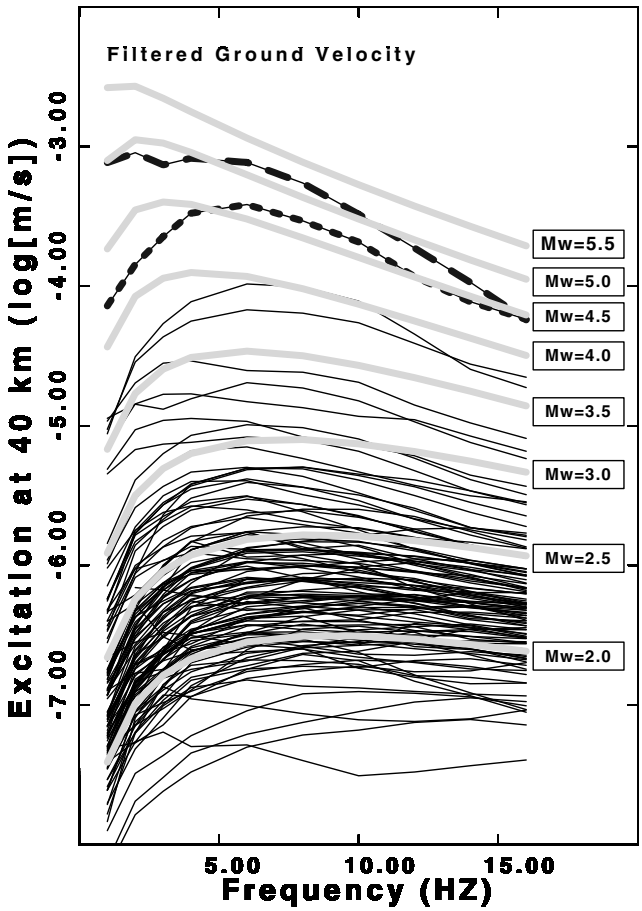

Figure 10. Filtered ground velocity excitation (thin black lines) and model-based prediction (thick gray lines) for the Utah region. The excitation terms are inverted from the combined vertical and horizontal data sets. The thin black line linked by the thick long-dashed line is the observed excitation of the Idaho earthquake and the thin black line linked by the thick short-dashed line is the excitation of the $\mathbf{M_W}$ 4.5 event.

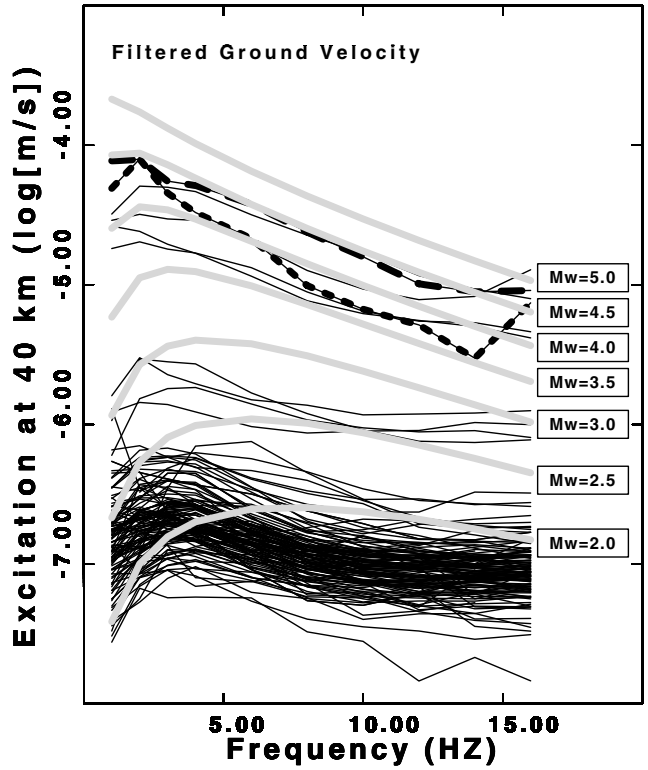

Figure 11. Mining-associated excitation of filtered ground velocity at 40 km. The excitation terms are for the combined vertical and horizontal data sets. The thick gray curves are the predictions from the 10-bar stress drops. The thin black line linked by thin and thick dashes indicates the excitation spectra of $\mathbf{M_W}$ 4.1 and $\mathbf{M_W}$ 4.2.

Table 3

Focal Mechanism Parameters

Date (yy/mm/dd)	Lat. (N°)	Long. (W°)	Strike (°)	Dip (°)	Rake (°)	Depth (km)	$\mathbf{M_W}$
98/01/02	38.18	112.46	235	50	20	16.0	4.52
00/01/30	41.52	109.81	30	75	80	7.0	4.10
01/04/21	42.92	111.39	355	30	−100	10.0	5.20
01/07/19	38.73	111.52	30	70	−100	2.0	4.23

Lat. and Long. denote latitude and longitude. Details on the determination of the source parameters can be found at www.eas.slu.edu/Earthquake_Center/NEW/mechanism.html

of Utah $\mathbf{M_L}$ values for these events. Perhaps the duration magnitude scale used for Yellowstone overestimates event sizes by an order of one magnitude unit (J. Pechmann, personal comm., 2003). An alternative explanation is that the $R_{\Theta\Phi}$ differs (Herrmann and Malagnini, 2004). This can be resolved only by waiting for a large-calibration event. Table 4 completes the specification of the spectral model used to predict the excitation terms for the Utah and Yellowstone regions.

Discussion

We estimated regional ground motion scaling relations for the seismically hazardous Wasatch front in the northeastern Basin and Range province and the Yellowstone region, which lies at the intersection of the eastern boundary of the Basin and Range tectonic province and the eastern Snake River Plain. Three-component velocity seismograms from the University of Utah seismogram seismic network were used to measure and quantify the regional attenuation ground motion. The distance scaling of Fourier velocity spectra and bandpass-filtered time domain peak motion were obtained for frequency ranges between 1.0 and 16.0 Hz. The regression results for Utah display consistent shapes, whereas rapid decay of amplitude with distance occurred at short distances. The crustal propagation term was modeled by a rapid geometrical spreading function at short distance ranges and a crustal attenuation parameter [$Q(f) = 160f^{0.75}$].

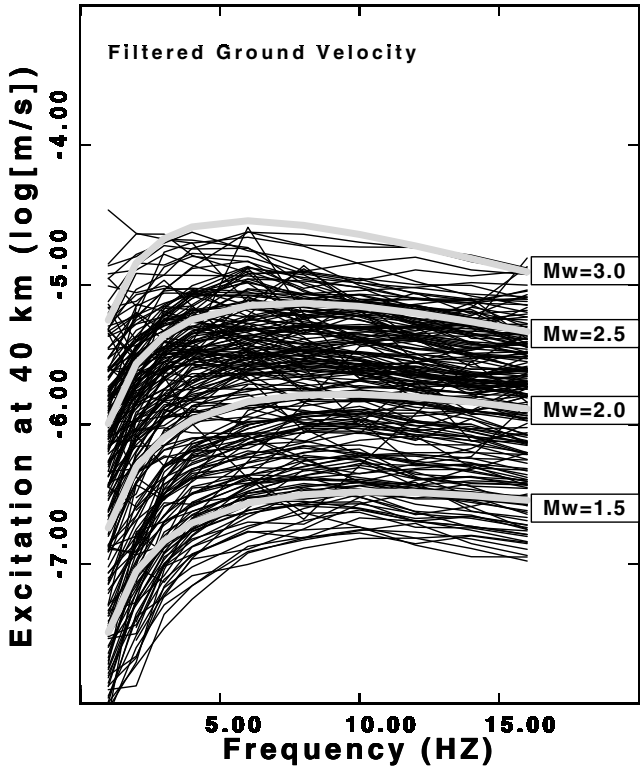

Figure 12. Filtered ground velocity excitation terms for the Yellowstone region superimposed by theoretical curves (thick gray lines) plotted on a linear frequency scale. The excitation terms are inverted from the combined vertical and horizontal motion data sets.

Table 4
Spectral Parameters of Utah and Yellowstone

Parameter	Numerical Value
ρ	2.8 g/cm^3
β	3.5 km/sec
f_c	$4.9 \times 10^6\ \beta\ (\Delta\sigma/M_0)^{1/3}$ Hz
M_0	$10^{1.5\mathbf{M_W}+16.05}$
$\Delta\sigma$	300 bars (Utah)
	30 bars (Yellowstone)
κ_{eff}	0.050 sec (Utah)
	0.040 sec (Yellowstone)

The rapid decrease of amplitude versus distance and low Q may mean that the probabilistic hazard analysis estimates for Utah will be controlled by local seismic events. The excitation of mining-associated events differs from earthquake excitation spectra by a rapid reduction in high-frequency excitation spectra.

We also carried out a quantitative analysis of the ground motion scaling in the Yellowstone region. One of the most important reasons for studying Yellowstone was to check if the $D(r, f)$ of Utah at short distance range differs from that of Yellowstone. Figure 3 indicates that the Yellowstone data set is large enough to check the validity of $D(r, f)$ at short distance ranges. The propagation functional was modeled by geometrical spreading less than $r^{-1.0}$ at a short distance range and a crustal parameter $Q(f) = 140f^{0.70}$. We used $\kappa_{\text{eff}} = 0.040$ sec and $\Delta\sigma = 30$ bars to predict the theoretical excitation spectra. Although many studies have been performed using the stochastic method technique, only the Yellowstone study result showed the $g(r)$ less than $r^{-1.0}$ at a short distance range and rapid falloff of $D(r, f)$ at mid-distance range (40–105 km).

The $Q(f) = 140f^{0.70}$ of the Yellowstone region reflects the average attenuation of the whole Yellowstone upper crust, inside and outside caldera. Clawson *et al.* (1989) showed that the surface layer (up to 2 km) has low Q (less than 50) in Yellowstone. The Q values in the upper crust, at depths ranging from 2 to 12 km, vary from 40 to 200 within the caldera, whereas Q values outside the caldera are greater than 200 because the upper crust is less affected by high temperatures and thermal alteration. The apparent Q at high frequencies in the crust is affected by thermal, anelastic, and scattering processes. Factors such as temperature, the amount of fluid content, and partial melt or solid-state dislocation motion in the crust or upper mantle affect the attenuation parameter Q (Mitchell, 1995).

Tables 1, 2, and 4 provide the parameters of our working model for predicting high-frequency peak ground motion using random vibration theory. We found differences in ground motion scaling between Utah and Yellowstone in the different $g(r)$ and $Q(f)$ functions. We cannot compare expected absolute motions for the same $\mathbf{M_W}$ for the two regions because we did not have a calibration event in the current Yellowstone data set.

Because our forward model was based on a trial-and-error fit of the data, we do not provide any error estimates on the individual parameters. This is because of the interdependence of the $g(r)$ and $Q(f)$ values, and because we have taken care to document the errors inherent in the regression estimates of the $D(r)$, $E(r_{\text{ref}}, f)$, and $S(f)$ terms. We believe that the distance dependence is understood for the two regions studied. The question of source spectrum scaling can only be addressed as data from larger events are patiently acquired.

Acknowledgments

We are grateful to Dr. James Pechmann and Sue Nava of the University of Utah for providing the excellent data set for this study and improving this manuscript. We thank Dr. Luca Malagnini for his critical reviews and Dr. Keith Koper for his comments about this article. We benefited from the thoughtful reviews of Drs. Martha Savage, Harley Benz, and James Pechmann and the suggestions of Associate Editor Dr. Art McGarr. Figure 1 was produced using the Generic Mapping Tools (Wessel and Smith, 1995). This research was partially supported the USGS National Earthquake Hazards Reduction Program Grant 02HQPA0001 and Mid-America Earthquake Center under Grant EEC-9701785 of the National Science Foundation for the Earthquake Engineering Research Centers program.

References

Aki, K. (1980). Scattering and attenuation of shear waves in the lithosphere, *J. Geophys. Res.* **85,** 6496–6504.

Akinci, A., L. Malagnini, R. B. Herrmann, N. A. Pino, L. Scognamiglio, and H. Eyidogan (2001). High-frequency ground motion in the Erzincan region, Turkey: inferences from small earthquakes, *Bull. Seism. Soc. Am.* **91,** 1446–1455.

Anderson, J. G., and Y. Lei (1994). Non-parametric description of peak acceleration as a function of magnitude, distance, and site in Guerrero, Mexico, *Bull. Seism. Soc. Am.* **84,** 1003–1017.

Arabasz, W. J., J. C. Pechmann, and E. D. Brown (1992). Observational seismology and the evaluation of earthquake hazards and risk in the Wasatch front area, Utah, in *Assessment of Regional Earthquake Hazards and Risk Along the Wasatch Front, Utah*, P. L. Gori and W. W. Hays (Editors), *U.S. Geol. Surv. Profess. Pap. 1500-A-J*, D1–D36.

Atkinson, G. (1993). Source spectra for earthquakes in eastern North America, *Bull. Seism. Soc. Am.* **83,** 1778–1798.

Atkinson, G. (2004). Empirical attenuation of ground motion spectral amplitudes in southeastern Canada and the northeastern United States (submitted for publication).

Atkinson, G., and W. Silva (1997). Empirical source spectra for California earthquakes, *Bull. Seism. Soc. Am.* **87,** 97–113.

Beresnev, I., and G. Atkinson (1997). Modeling finite-fault radiation from the ω^n spectrum, *Bull. Seism. Soc. Am.* **87,** 67–84.

Beresnev, I. A., and G. M. Atkinson (1998). FINSIM-a FORTRAN program for simulating stochastic acceleration time histories form finite faults, *Seism. Res. Lett.* **69,** 27–32.

Beresnev, I. A., and G. M. Atkinson (1999). Generic finite-fault model for ground motion prediction in Eastern North America, *Bull. Seism. Soc. Am.* **89,** 608–625.

Best, M. G., and W. H. Brimhall (1974). Late Cenozoic alkalic basaltic magmas in the western Colorado plateaus and the Basin and Range transition zone, U.S.A., and their bearing on mantle dynamics, *Geol. Soc. Am. Bull.* **85,** 1677–1690.

Boatwright, J., and G. Choy (1992). Acceleration source spectra anticipated for large earthquakes in eastern North America, *Bull. Seism. Soc. Am.* **82,** 660–752.

Boore, D. M. (1983). Stochastic simulation of high-frequency ground motion based on seismological models of the radiated spectra, *Bull. Seism. Soc. Am.* **73,** 1865–1894.

Boore, D. M. (2003). Prediction of ground motion using the stochastic method, *Aki Symposium, Pageoph* **160,** 635–676.

Cartwright, D. E., and M. S. Longuet-Higgins (1956). The statistical distribution of the maxima of a random function, *Proc. R. Soc. London A* **237,** 212–232.

Centroid Moment Tensor (CMT) Catalog, www.seismology.harvard.edu/CMTsearch.html (last accessed August 2003).

Christiansen, R. L. (2001). Geology of Yellowstone National Park, The Quaternary and Pliocene Yellowstone plateau volcanic field of Wyoming, Idaho and Montana, *U.S. Geol. Surv. Profess. Pap. 729-G.*

Clawson, S. R., R. B. Smith, and H. M. Benz (1989). P wave attenuation of the Yellowstone Caldera from three-dimensional inversion of spectral decay using explosion source seismic data, *J. Geophys. Res.* **94,** 7205–7222.

Frankel, A., J. McGarr, J. Bicknell, L. Mori, L. Seeber, and E. Cranswick (1990). Attenuation of high-frequency shear waves in the crust; Measurements from New York state, South Africa, and Southern California, *J. Geophys. Res.* **95,** 17,441–17,457.

Harmsen, S. (1997). Estimating the diminution of shear-wave amplitude with distance: application to the Los Angeles, California, urban area, *Bull. Seism. Soc. Am.* **87,** 888–903.

Herrmann, R. B. (1979). Surface wave focal mechanisms for eastern North American earthquakes with tectonic implications, *J. Geophys. Res.* **84,** 3543–3552.

Herrmann, R. B. (1985). An extension of random vibration theory estimates of strong ground motion to large distances, *Bull. Seism. Soc. Am.* **75,** 1447–1453.

Herrmann, R. B., and J. Dutt (1999). High frequency vertical ground motion in the Pacific Northwest using PNSN data, *Seism. Res. Lett.* **70,** 216.

Herrmann, R. B., and L. Malagnini (1996). Absolute ground motion scaling in the New Madrid Seismic Zone, *Seism. Res. Lett.* **67,** 40.

Herrmann, R. B., and L. Malagnini (2004). Interpretation of high frequency ground motion from regional seismic network observations (submitted for publication).

Lawson, C. L., and R. J. Hanson (1974). *Solving Least Squares Problems*, Prentice-Hall, Englewood Cliffs, New Jersey.

Machette, M. N., S. F. Personius, A. R. Nelson, D. P. Schwartz, and W. R. Lund (1991). The Wasatch fault zone, Utah-segmentation and history of Holocene earthquakes, *J. Struct. Geol.* **13,** 137–149.

Malagnini, L., and R. B. Herrmann (2000). Ground motion scaling in the region of the 1997 Umbria-Marche earthquake (Italy), *Bull. Seism. Soc. Am.* **90,** 1041–1051.

Malagnini, L., R. B. Herrmann, and M. Di Bona (2000a). Ground motion scaling in the Apennines (Italy), *Bull. Seism. Soc. Am.* **90,** 1062–1081.

Malagnini, L., R. B. Herrmann, and K. Koch (2000b). Regional ground motion in scaling in Central Europe, *Bull. Seism. Soc. Am.* **90,** 1052–1061.

McCalpin, J. P., and S. P. Nishenko (1996). Holocene paleoseismicity, temporal clustering, and probabilities of future large ($M > 7$) earthquakes on the Wasatch fault zone, Utah, *J. Geophys. Res.* **101,** 6233–6253.

Miller, D. S., and R. B. Smith (1999). P and S velocity structure of the Yellowstone volcanic field from local earthquake and controlled-source tomography, *J. Geophys. Res.* **104,** 15,105–15,121.

Mitchell, B. J. (1995). Anelastic structure and evolution of the continental crust and upper mantle from seismic surface wave attenuation, *Rev. Geophys.* **33,** 441–462.

Ortega, R., R. B. Herrmann, and L. Quintanar (2003). Earthquake ground-motion scaling in Central Mexico between 0.7 and 7 Hz, *Bull. Seism. Soc. Am.* **93,** 397–413.

Pechmann, J. C., W. R. Walter, S. J. Nava, and W. J. Arabasz (1995). The February 3, 1995, M_L 5.1 seismic event in the Trona mining district of southwestern Wyoming, *Seism. Res. Lett.* **66,** no. 3, 25–34.

Pino, N. A., L. Malagnini, A. Akinci, L. Scognamiglio, R. B. Herrmann, G. Stavrakakis, and G. Chouliaras (2001). Ground motion scaling relationships for mainland Greece and Crete, *Seism. Res. Lett.* **72,** 258.

Raoof, M., R. B. Herrmann, and L. Malagnini (1999). Attenuation and excitation of three-component ground motion in Southern California, *Bull. Seism. Soc. Am.* **89,** 888–902.

Saint Louis University earthquake center home page, www.eas.slu.edu/Earthquake_Center/NEW/mechanism.html (last accessed April 2004).

Smith, R. B., and W. J. Arabasz (1991). Seismicity of the Intermountain seismic belt, in *Neotectonics of North America*, D. B. Slemmons, E. R. Engdahl, M. D. Zoback, and D. D. Blackwell (Editors), Geol. Soc. Am. Decade Map Vol. I, 185–228.

Wessel, P., and W. H. F. Smith (1995). New version of the Generic Mapping Tools released, *EOS Trans. Am. Geophys. Union* **76,** 329.

Yazd, M. R. S. (1993). Ground motion studies in the Southern Great Basin of Nevada and California, *Ph.D. Thesis*, Saint Louis University.

Department of Earth and Atmospheric Sciences
Saint Louis University
3507 Laclede Avenue
St. Louis, Missouri 63103
sooy@eas.slu.edu
rbh@eas.slu.edu

Manuscript received 24 October 2003.